CVD diamond growth from nanodiamond seeds buried under a thin chromium layer

Reference:

Degutis G., Pobedinskas P., Turner Stuart, Lu Yinggang, Verbeeck Johan, et al..- CVD diamond growth from nanodiamond seeds buried under a thin chromium layer

Diamond and related materials - ISSN 0925-9635 - 64(2016), p. 163-168

Full text (Publishers DOI): http://dx.doi.org/doi:10.1016/j.diamond.2016.02.013

CVD diamond growth from nanodiamond seeds buried under a thin chromium layer

G. Degutis,[1 a)] P. Pobedinskas,[1,2] S. Turner,[3] Y.-G. Lu,[3] S. Al Riyami,[1,4,5] B. Ruttens[2], T. Yoshitake,[4] J. D'Haen,[2] K. Haenen,[1,2] J. Verbeeck,[3] A. Hardy,[1,2] and M.K. Van Bael,[1,2]

[1)] Institute for Materials Research (IMO), Hasselt University, B-3500 Hasselt, Belgium

[2)] IMOMEC, IMEC vzw, B-3590 Diepenbeek, Belgium

[3)] EMAT, University of Antwerp, B-2020 Antwerp, Belgium

[4)] Kyushu University, 6-1 Kasuga, Fukuoka 816-8580, Japan

[5)] German University of Technology in Oman, Barka, Sultanate of Oman

Highlights

- Carbon diffusion into the Cr layer during the early CVD diamond growth stages
- Carburization and salicidation of the Cr layer in the high-temperature, H-rich plasma
- Study of the local diamond environment evolution at the Si/Cr interface

Abstract

This work presents a morphological and structural analysis of CVD diamond growth on silicon from nanodiamond seeds covered by a 50 nm thick chromium layer. The role of carbon diffusion as well as chromium and carbon silicide formation is analyzed. The local diamond environment is investigated by scanning transmission electron microscopy in combination with electron energy-loss spectroscopy. The evolution of the diamond phase composition (sp^3/sp^2) is evaluated by micro-Raman spectroscopy. Raman and X-ray diffraction analysis are used to identify the interfacial phases formed during CVD growth. Based upon the observed morphological and structural evolution, a growth model for diamond from nanodiamond seeds buried beneath a thin Cr layer is proposed.

Keywords: CVD diamond, Cr diffusion, Cr carburization, Si-Cr interface.

1. Introduction

For many years, silicon has been the substrate of choice in the microelectronics industry, and its application remains a major research field, especially in conjunction with other materials. Chromium is usually used as an adhesive layer for less adhesive materials, like gold, and therefore Cr diffusion reactions have been widely studied in

the past [1]. It is known that Cr tends to diffuse and react with the substrate during processing, depending upon the choice of substrate and other combined materials. For example, in NEMS/MEMS [2,3] or CMOS structures [4], the behavior of the Cr interlayers during the processing steps is of fundamental importance [5-7]. Recently, it was shown that thermionic emission properties can be improved by employing chromium silicide (Cr_5Si_3) as an electrical nanocontact material, as it facilitates charge transfer through the Si/Au interface by lowering the Schottky barrier [8].

During chemical vapor deposition (CVD) of diamond, refractory metals (including Cr) are susceptible to fast carburization [9]. Generally, Cr can form three forms of stable carbide, i.e., Cr_3C_2, Cr_7C_3, and $Cr_{23}C_6$ [10]. The carburization process is intrinsically important to the metallurgical and microelectronics industry, meaning the kinetics of carbide formation have been thoroughly investigated in the literature [11]. For its intrinsic properties Cr can also be used as a diffusion barrier layer during CVD growth of diamond on foreign substrates containing ferrous metals like Fe, Ni and Co [12]. These ferrous metals are known to catalytically assist conversion of CVD deposited sp^3 carbon to sp^2 graphitic carbon [13], which is detrimental to diamond coating adhesion on alloys (e.g., WC-Co) containing those constituent components. Thus the application of a carbon in-diffusion barrier layer like Cr is necessary. Here, a thin Cr barrier layer serves as sacrificial layer and simultaneously acts as carburized nucleation layer for diamond growth [14].

CVD diamond, being a unique material bearing outstanding intrinsic properties, is of great potential interest for optoelectronic high-power, high-temperature and high-frequency devices [15-17].The performance of such devices is sensitive to the properties of the materials as well as to the interfaces that emerge during processing. Recently, an interest towards investigation of bright Cr color centres that are present in diamond has risen, with a new challenging aim to incorporate Cr into a diamond lattice in controlled manner [18,19].

Therefore, in this work, we aim to investigate the local diamond environment as well as interfacial compounds that form during the early CVD growth stages of diamond on a Cr-covered Si substrate. The focus lies on the analysis of the interaction between the thin Cr layer and the hydrocarbon species from the CVD plasma, as well as silicide formation. We use an approach where CVD diamond is grown from nanodiamond (ND) seeds buried under a thin Cr layer. This provides the advantage of achieving a high seeding density of ND on Si [20], which would be difficult to realize on Cr [12,21,22]. Such an approach was recently demonstrated in the case of a Pt over-layer for adhesion improvement on Cu [23]. We thoroughly examine the growth of the nanocrystalline (NCD) layer and suggest a model to explain the diamond growth mechanism in this case.

2. Experimental

Highly resistive silicon (10-20 kΩcm) substrates were wet-cleaned using a standard silicon cleaning procedure; they were first immersed into a hot sulphuric acid (H_2SO_4, 95%) and hydrogen peroxide (H_2O_2, 30%) mixture (4:1, 120 °C), and afterwards in an ammonium hydroxide (NH_4OH, 28%), H_2O_2 and a DI water mixture (1:1:5, 80 °C) for 20 min per bath. The substrates were then rinsed with DI water and dried under a nitrogen gas flow. Detonation ND powder was acquired from the NanoCarbon Institute Co., Ltd., Japan. This powder was dispersed in DI water using a high-power

ultrasonic horn [20]. The particle size distribution proved to contain of approximately 7 nm ND in diameter and the zeta-potential is (49±5) mV at pH 4.8 was determined by dynamic light scattering (DLS) using photon correlation spectroscopy with a ZetaPALS90Plus/BI-MAS Particle Sizing Option (Brookhaven Instruments Corporation).

The cleaned substrates were dipped in a ND suspension for 2 min and then rinsed with DI water on a spin-coater at 4000 rpm and dried. Afterwards, the substrates seeded with ND were coated with 50 nm of Cr by pulsed direct current magnetron sputtering [21]. The target power supply was driven in constant-power mode at 150 W. An argon gas flow of 50 sccm was fixed by a mass flow controller and a gas pressure of 0.4 Pa was kept constant during the deposition. The distance between the target and the substrate was 12 cm.

NCD films were grown by microwave plasma enhanced CVD (MW PE CVD) in an ASTeX 6500 reactor using the following growth conditions: 3% (15 sccm flow) of methane diluted by hydrogen (485 sccm), 3500 W microwave power and 3.3×10^4 Pa process pressure sustained 730 °C substrate temperature. NCD growth was initiated for various times from 3 min to 96 min.

The samples after the CVD step where characterized by Raman spectroscopy. The spectra were recorded by a Horiba Jobin-Yvon T64000 spectrometer equipped with a confocal microscope. Excitation of the samples was performed with an Ar^+-ion 488 nm laser (Lexel SHG-95). The laser power was attenuated to avoid sample heating using an appropriate neutral density filter. Scanning electron microscopy (SEM) was acquired on a FEI Quanta 200 FEG-SEM. Structural characterisation of the CVD plasma exposed samples was performed by X-ray diffraction (XRD), using the Cu-$K_{\alpha 1}$ line (λ = 0.154056 nm) on a Siemens D5000 Bragg-Brentano diffractometer.

A 24 min CVD growth sample was prepared by a focused ion beam lift-out procedure in a FEI Helios FIB-SEM for cross-sectional examination by scanning transmission electron microscopy (STEM). High-angle annular dark field (HAADF) images and electron energy loss spectra (EELS) were acquired using an aberration corrected FEI Titan 80-300 “cubed” microscope equipped with a GIF Quantum spectrometer, operated at 120 kV. A convergence semi-angle of 22 mrad and an acceptance angle of 46 mrad were used. The STEM-EELS $CrSi_2$ map was generated using a multiple least squares fitting of a $CrSi_2$ Si $L_{2,3}$ reference spectrum to the Si $L_{2,3}$ edge in each spectrum of the acquired EELS.

3. Results and discussion

3.1 Morphological changes

SEM overview images were recorded after varying diamond CVD synthesis times to compare the structural change in surface morphology of the nucleating NCD film with and without the presence of a Cr layer (Figs. 1(a) and 1(b)). Additionally, to evaluate the influence of the very hydrogen-rich CVD plasma on the Cr layer, a sample containing only a Cr layer was placed in each CVD run (Fig. 1(c)). The first diamond nucleus appears on the Cr surface after 12 min of exposure to the CVD plasma (Fig. 1(b), indicated with arrows), whereas at this time the reference sample without a Cr coating already shows the presence of a homogeneous, coalesced NCD thin film (Fig. 1(a)). After 24 min, more sparsely scattered grains appear on top of the Cr layer and it can be seen that the diamonds have also started to grow in the lateral

directions. After 96 min, due to lateral growth, the diamond crystals have expanded, forming a coalesced diamond film on top of the Cr layer with much larger crystallites than on the uncovered seeded Si substrate. The observed difference in diamond crystallite sizes is a result of the different number of ND seeds accessible to plasma species during the NCD growth.

In parallel, the morphological changes occurring in the Cr layer without buried NDs are traced (Fig. 1(c)). It is clearly visible that even at an early CVD stage (< 12 min) microscopic cracks have started to appear in both Cr layers, with and without NDs. These cracks (Fig. 1(c), indicated by arrows) appear due to the influence of the plasma; carbon diffuses into the Cr layer and forms $Cr_{23}C_6$, which is confirmed by a detailed TEM analysis (Sec. 3.3). These gradually appearing defects act as diffusion channels: carbon radicals from the CVD plasma can access the uncovered NDs, leading to the initiation of diamond growth at these places after longer exposure to the plasma. It is likely that the appearance of microscopic fracturing is being enhanced by an ongoing concurrent chemical reaction, i.e., the thermally driven diffusion of Cr into Si. This leads to the formation of $CrSi_2$, which is confirmed by Raman analysis, (Sec. 3.2.). A similar $CrSi_2$ formation was observed by Bower *et al*. [24]. Furthermore, Olowolafe *et al*. studied the temperature dependent formation kinetics of $CrSi_2$ thoroughly and revealed that this process is thermally activated with an activation energy of (1.7 ± 0.1) eV [6]. In our case, after CVD plasma exposure, the layer gradually shrinks from a smooth and homogeneous one to textured $Cr_{23}C_6$ domains.

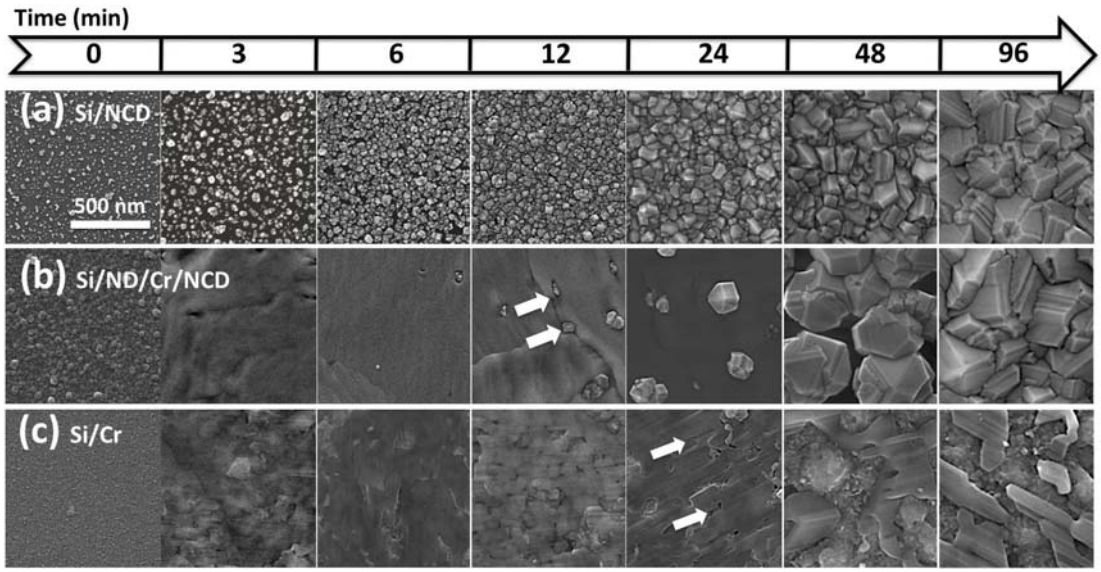

Fig. 1. SEM micrographs of the (a) normal growth of NCD on Si, (b) NCD growth from NDs buried under a 50 nm Cr layer, and (c) Cr on Si exposed to CH_4/H_2 plasma.

Micro-Raman spectroscopy was used for the quality evaluation of the NCD films [25]. As a measure of diamond film quality, the fraction of graphitic sp^2 carbon is evaluated in the Raman spectra, which directly provides information on the various carbon forms present in the samples. Features arising due to sp^2 sites upon excitation with a visible laser have scattering cross-sections that are roughly 50-230 times higher than those due to sp^3 excited states [26]. This makes visible light excited Raman spectroscopy a perfect characterization method to extract information about the

presence of non-diamond carbon phases and therefore a direct method to evaluate diamond quality.

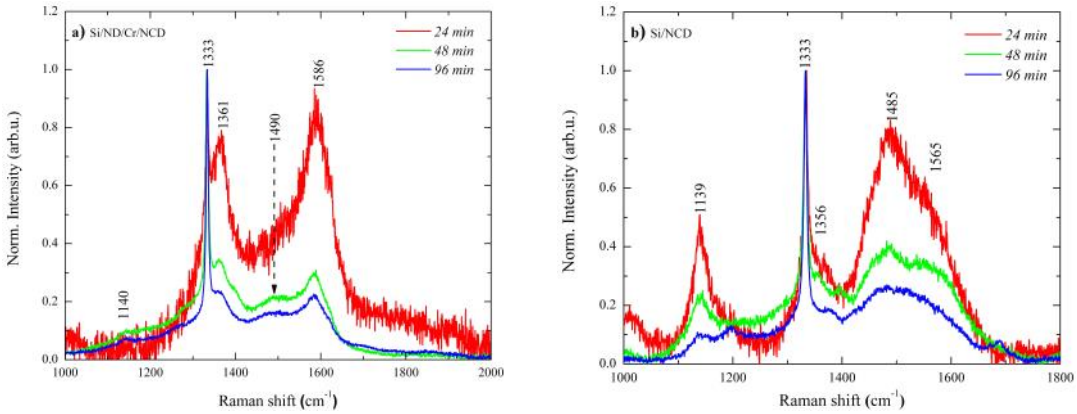

Fig. 2. Background subtracted Raman spectra (normalized to diamond 1332 cm^{-1} peak) of NCD varying with CVD growth time for (a) Si/ND/Cr/NCD and (b) Si/NCD.

Figure 2 shows that the background subtracted Raman spectra vary with CVD growth time on both experimental configurations. The spectra are normalized to the sp^3 diamond peak (1333 cm^{-1}). The slight of shift from the stress-free 1332 cm^{-1} phonon position can be attributed to the residual stress present in the films [25]. The Raman spectra indicate the growth of high quality, i.e., relatively low sp^2 content NCD films. In both cases, the sp^3/sp^2 ratio increases with deposition time. The characteristic graphitic carbon feature, the so-called G-band present at 1586 cm^{-1} for Si/ND/Cr/NCD and 1565 cm^{-1} for Si/NCD, which decreases with growth time, is indicating an improvement of the diamond film quality at longer CVD growth. The Raman spectra of the shorter growth times (up to 12 min) are not shown for comparison due to the absence of the diamond phonon in the case of Si/ND/Cr/NCD configuration. The presence of a feature at 1139 cm^{-1} in Si/NCD is assigned to -CH_x bonds and the feature at 1490 cm^{-1} can be tentatively ascribed to sp^2 carbon located in the grain boundaries [26]. The data show that the Si/NCD films have a slightly higher content of sp^2 carbon than the Si/ND/Cr/NCD films. This can be understood by the fact that the diamond crystallites grown on Si are smaller in size, meaning a relatively higher amount of grain boundaries, as compared to the Si/ND/Cr/NCD samples, where the diamond crystallites are larger with less grain boundary material (Figs. 1(a) and 1(b), 48 min and 96 min).

3.2 Compositional changes

To understand ongoing compositional changes at the Si/Cr interface during the CVD process, micro-Raman spectra were measured in the range between 250 cm^{-1} and 900 cm^{-1} in order to trace potentially formed silicide and carbide compounds (Fig. 3). After 12 min of plasma exposure, phonon modes at 302 cm^{-1}, 349 cm^{-1}, 390 cm^{-1} and 409 cm^{-1} appear. These peaks are in a good agreement with those belonging to $CrSi_2$ reported in literature [27]. One can note that the Si phonon mode at 520.7 cm^{-1} gradually appears with CVD exposure time. This could be explained by the fact that the laser beam does not reach the substrate until the carburized Cr layer begins to fracture during CVD growth. The same implication is valid for $CrSi_2$. The increased intensities of the characteristic $CrSi_2$ phonons hint at the fact that the amount of

crystalline $CrSi_2$ increases. A small skewed signal, arising after 96 min at ~790 cm^{-1}, belongs to the SiC present in a minute amount at the Si interface [28]. This is a common interfacial alloy, formed during the diamond CVD process.

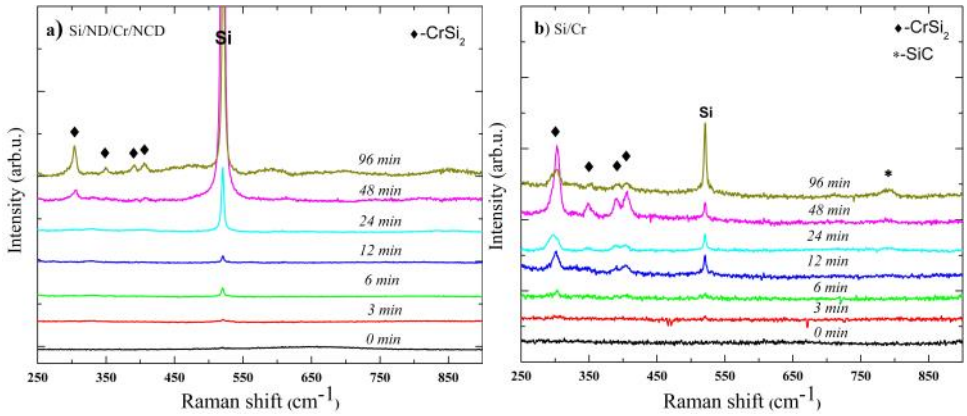

Fig. 3. Raman spectra of (a) ND on Si covered with Cr and (b) Si covered with Cr as a function of exposure time to CVD plasma.

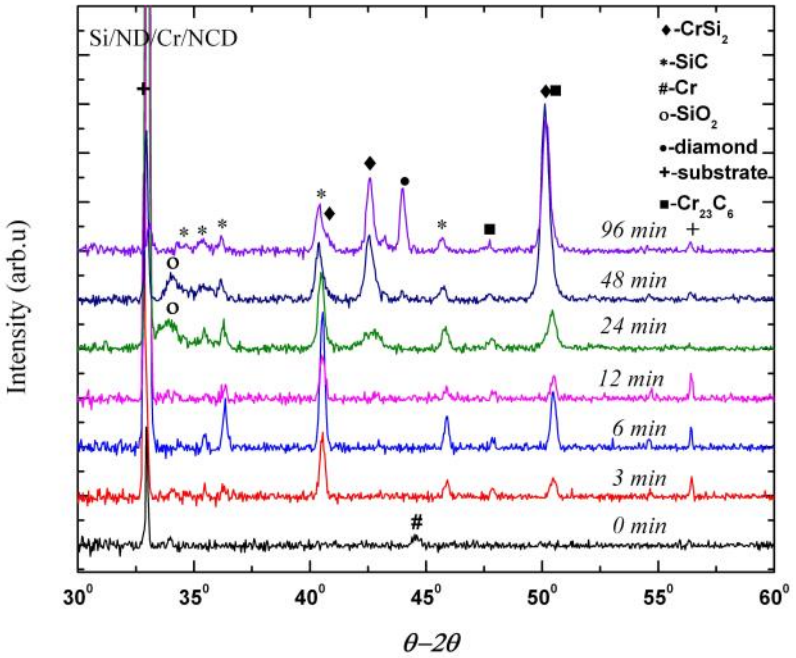

Fig. 4. XRD patterns of the Si/ND/Cr/NCD samples.

The XRD patterns depicted in Fig. 4 are in a good agreement with the Raman data. The diffraction patterns reveal that, even after a very short exposure of the Cr coating to the CVD plasma, the metal layer is fully converted to carbide and silicide. The latter was confirmed by TEM, where no metallic Cr was observed for the 24 min Si/ND/Cr/NCD grown sample. As is evident from the XRD of the 3 min growth sample, the presence of SiC indicates that the Cr layer becomes saturated with carbon at the initial stage. The carbon (CH_x) species come from the methane containing plasma, which is needed for carbide formation at the Si/Cr interface. The two peaks

observed at 47.8° and 50.1° are assigned to the (440) and (531) reflections, respectively, of the $Cr_{23}C_6$ carbide phase [29]. The XRD pattern also confirms the rapid formation of the $CrSi_2$ phase, which is the only Cr_xSi_y phase detected, consistent with Raman spectroscopy.

3.3 Local environment investigation of the diamond crystallites /Cr interface by TEM

Combining mass-thickness sensitive HAADF-STEM imaging with spatially resolved EELS should provide a better understanding of the presence and distribution of the various phases in the sample, after the substantial Si/Cr interfacial diffusion and carbon inter-diffusion into the Cr layer have occurred. To this end, the Si/ND/Cr/NCD sample after 24 min of CVD growth was prepared in cross-section by a focused ion beam lift-out procedure (Fig. 5). The HAADF-STEM images in Figs. 5(a) and 5(b) show an overview of the sample. The dark-contrast regions in the bright layer are diamond grains that have started to form. The high resolution HAADF-STEM image and inset Fourier transform pattern in (Fig. 5(c)) demonstrate that the initial Cr layer deposited on top of the NDs is fully carburized, as the structure fully coincides with the $Cr_{23}C_6$ carbide phase. The EELS spectrum confirms that the Cr layer is not metallic, but contains a significant amount of carbon (Fig. 5(d)). This supplements the XRD data that the previous Cr layer no longer shows the presence of metallic Cr after 3 min of CVD. This, therefore, allows us to conclude that Cr rapidly carburizes in the 3% CH_4 concentration plasma. This is further supported by the immediate formation of SiC, for which carbon must be in contact with Si.

The $Cr_{23}C_6$ layer appears to have cracked open, where the diamond grain formation has occurred. It then seems that the diamond grains do not spontaneously nucleate on top of the $Cr_{23}C_6$ surface, but rather grow from the uncovered diamond seeds. The higher magnification image (Fig. 5(b)) also shows bright-contrast regions embedded in the Si substrate. These regions vary in size from approximately 10 nm to 40 nm. Using high-resolution imaging (not displayed here) and spatially resolved EELS mapping (Figs. 5(e) and (f)), the regions were identified as being $CrSi_2$ inclusions as indicated by Raman (Fig. 3(b)) and XRD (Fig. 4).

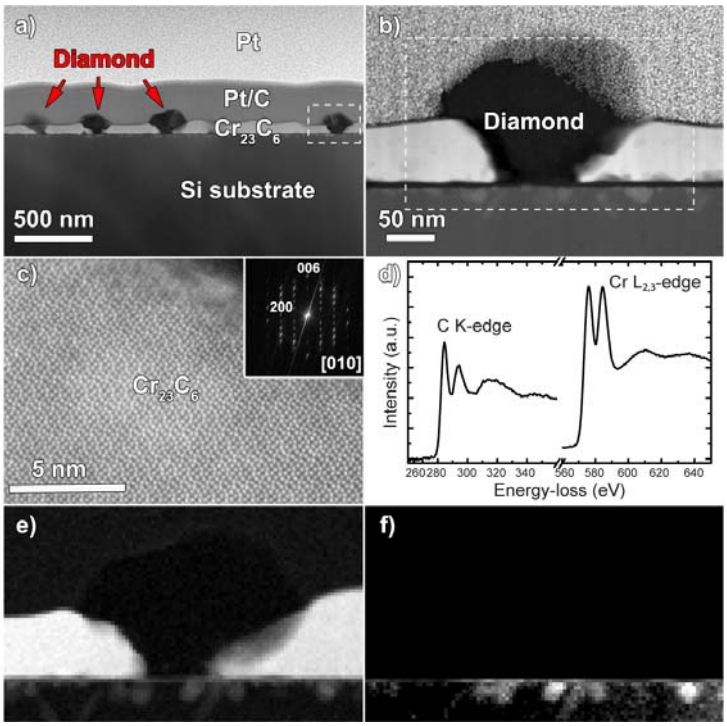

Fig. 5. (a) HAADF-STEM overview image of the Si/ND/Cr/NCD sample grown for the 24 min. (b) Enlarged area of a single diamond crystallite indicated by the dashed rectangle in (a). (c) High-resolution HAADF-STEM image of the $Cr_{23}C_6$ layer (former sputtered Cr layer), the inset Fourier transform pattern evidences the [010] zone axis orientation. (d) EELS spectrum, taken from $Cr_{23}C_6$ layer. (e) STEM-EELS Cr map from the region indicated by the dashed rectangle in (b), and (f) $CrSi_2$ map from the same region, indicated by the white rectangle in (b).

3.4 Model of diamond growth from buried NDs

Here, we propose a model of diamond nucleation and growth from a ND seeds buried beneath a Cr layer that acts as barrier layer between the ND and the CH_4 diluted in H_2 plasma. The early growth path can be sub-divided into four stages according to the morphological and structural changes of the Cr layer and step-by-step NCD film evolution observed here. Both processes are discussed in conjunction.

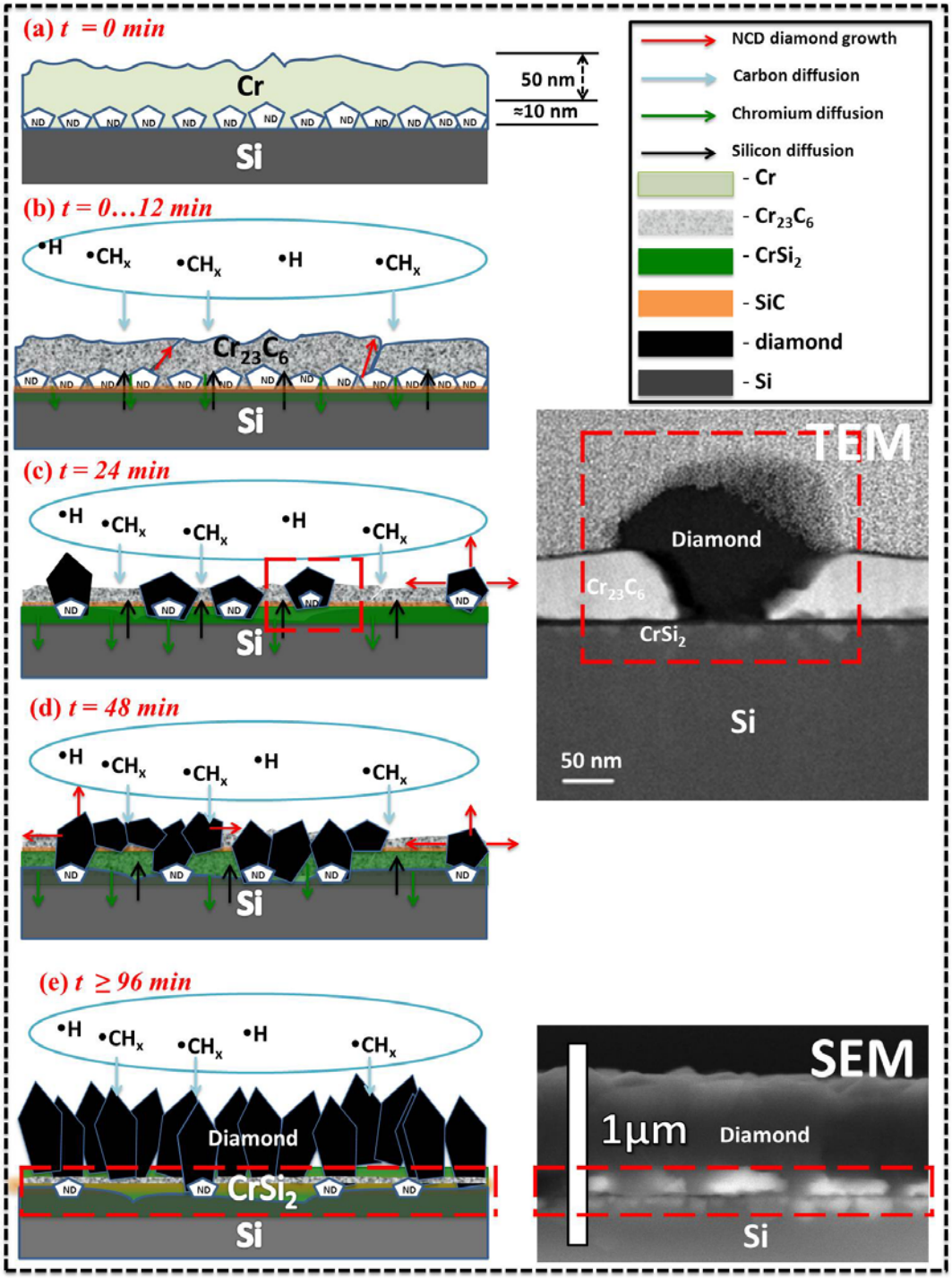

Fig. 6. Schematic illustration of the NCD growth through thin Cr layer.

t = 0 to 12 min (Fig. 6(b)): The thin Cr layer begins to fracture due to the thermally driven reaction of Cr with Si, which leads to the formation of $CrSi_2$. In parallel, the Cr layer carburizes due to the absorption of carbon from the plasma. As a consequence, carbon comes in contact with the Si substrate and forms SiC.

t = 12 to 24 min (Fig. 6(b-c)): As a consequence of the fracturing of the Cr carbide film, •H and •CH_x radicals can reach the previously buried NDs through microscopic channels (marked with red arrows, where the diamond growth occurs) in (Fig. 6(b)) and continue with hydrogen mediated NCD growth.

t = 48 min (Fig. 6(d)): At this stage the NCD continues to grow (axially and expands laterally on the $Cr_{23}C_6$ surface). Cr diffusion into Si and Si diffusion into Cr continues and the $Cr_{23}C_6$ layer starts to convert to $CrSi_2$.

t ≥ 96 min (Fig. 6(e)): Diamond growth continues like on Si and is dependent only on the species present in the plasma. Carbon ($\bullet CH_x$) bearing species emerging from the plasma are no longer in contact with the $Cr_{23}C_6$ and $CrSi_2$ layers.

5. Conclusions

In this study we have examined various aspects of nanocrystalline diamond growth from nanodiamond seeds buried under a 50 nm Cr layer on a Si substrate. We further focused on chemical reactions taking place at the Si/Cr interface during the CVD process. Based upon the observed results, a growth model was proposed. The importance of our model can be anticipated not only for the understanding of how the diamond grow through a thin Cr layer, but also to gain more insight into complex interfacial chemical reactions during the early stages of CVD growth. We suggest that the same growth model could be valid for other transition metals, bearing in mind their ability to form carbides and silicides simultaneously. Finally, we show that one can grow high quality NCD diamond on top of a Cr layer.

Acknowledgements

The authors acknowledge financial support provided by Research Programme FWO G.056.810. A.H. and M.K.V.B are grateful to Hercules Foundation Flanders for financial support. P.P. and S.T. are Postdoctoral Fellows of the Research Foundation – Flanders (FWO).

References

[1] M.A. Nicolet, Diffusion barriers in thin films, Thin Solid Films. 52 (1978) 415–443.

[2] V. Mulloni, R. Bartali, S. Colpo, F. Giacomozzi, N. Laidani, B. Margesin, Electrical and mechanical properties of layered gold–chromium thin films for ohmic contacts in RF-MEMS switches, Mater. Sci. Eng. B. 163 (2009) 199–203.

[3] V. Mulloni, J. Iannacci, R. Bartali, V. Micheli, S. Colpo, N. Laidani, et al., Gold-based thin multilayers for ohmic contacts in RF-MEMS switches, Microsyst. Technol. 18 (2012) 965–971.

[4] F. D'Heurle, Silicide Interfaces in Silicon Technology, J. Electron. Mater. 27 (1998) 1138–1147.

[5] H. Benkherbache, A. Merabet, Interdiffusion and growth of chromium silicide at the interface of Cr/Si(As) system during rapid thermal annealing, Thin Solid Films. 518 (2010) 2370–2373.

[6] J.O. Olowolafe, M. Nicolet, J.W. Mayer, Formation kinetics of $CrSi_2$ films on Si substrates with and without interposed Pd_2Si layer, J. Appl. Phys. 47 (1976) 5182–5186.

[7] W.-S. Lee, T.-Y. Liu, T.-H. Chen, Nanoindentation Behaviour and Microstructural Evolution of Au/Cr/Si Thin Films, Mater. Trans. 50 (2009) 1768–1777.

[8] M.-T. Chang, C.-Y. Chen, L.-J. Chou, L.-J. Chen, Core-shell chromium silicide-silicon nanopillars: a contact material for future nanosystems., ACS Nano. 3 (2009) 3776–80.

[9] H. Liu, D.S. Dandy, Studies on nucleation process in diamond CVD: an overview of recent developments, Diam. Relat. Mater. 4 (1995) 1173–1188.

[10] T. Massalski, Phase Diagrams in Materials Science, Metall. Trans. A. 20 (1989) 1295–1323.

[11] W.P. Leroy, C. Detavernier, R.L. Van Meirhaeghe, C. Lavoie, Thin film solid-state reactions forming carbides as contact materials for carbon-containing semiconductors, J. Appl. Phys. 101 (2007) 053714.

[12] M. Kawarada, K. Kurihara, K. Sasaki, Diamond synthesis on a metal substrate, Diam. Relat. Mater. 2 (1993) 1083–1089.

[13] R. Haubner, A. Lindlbauer, B. Lux, Diamond deposition on chromium, cobalt and nickel substrates by microwave plasma chemical vapour deposition, Diam. Relat. Mater. 2 (1993) 1505–1515.

[14] R. Haubner, W. Kalss, Diamond deposition on hardmetal substrates – Comparison of substrate pre-treatments and industrial applications, Int. J. Refract. Met. Hard Mater. 28 (2010) 475–483.

[15] Y. Yokoyama, X. Li, K. Sheng, A. Mihaila, T. Traikovic, F. Udrea, et al., A field effect transistor using highly nitrogen-doped CVD diamond for power device applications, Appl. Surf. Sci. 216 (2003) 483–489.

[16] D. Takeuchi, S. Koizumi, T. Makino, H. Kato, M. Ogura, H. Ohashi, et al., Negative electron affinity of diamond and its application to high voltage vacuum power switches, Phys. Status Solidi. 210 (2013) 1961–1975.

[17] R. J. Nemanich, J. A. Carlisle, A. Hirata and K. Haenen, CVD diamond-Research, applications, and challenges, MRS Bulettin. 39 (2014) 492-494.

[17] R.J. Trew, J.-B. Yan, P.M. Mock, The potential of diamond and SiC electronic devices for microwave and millimeter-wave power applications, Proc. IEEE. 79 (1991) 598–620.

[18] T. Müller, I. Aharonivich, Z. Wang, X. Yuan, S. Castelleto, S. Prawer and M. Atatüre, Phonon-induced dephasing of chromium color centres in diamond, Phys.Rev. B 86 (2012) 195210.

[19] T. Müller, I. Aharonivich, L. Lombez, Y. Alaverdyan, A. N.Vamivakas, S. Castelleto, F. Jelezko, J. Wrachtrup, S. Prawer and M. Atatüre, Wide-range electrical tunability of single-photon emission from chromium-based centres in diamond, New J. of Phys. 13 (2011) 075001.

[20] O.A. Williams, O. Douhéret, M. Daenen, K. Haenen, E. Õsawa, M. Takahashi, Enhanced diamond nucleation on monodispersed nanocrystalline diamond, Chem. Phys. Lett. 445 (2007) 255–258.

[21] G. Degutis, P. Pobedinskas, H.-G. Boyen, W. Dexters, W. Janssen, S. Drijkoningen, A. Hardy, K. Haenen, M.K. Van Bael, Improved nanodiamond

seeding on chromium by surface plasma pretreatment, Chem. Phys. Lett. xx (2015) xx.

[22] Y.K. Chou, J. Liu, CVD diamond tool performance in metal matrix composite machining, Surf. Coatings Technol. 200 (2005) 1872–1878.

[23] X. Liu, Q. Wei, Z. Yu, T. Yang, H. Zhai, Adherent diamond film deposited on Cu substrate by carbon transport from nanodiamond buried under Pt interlayer, Appl. Surf. Sci. 265 (2013) 714–719.

[24] R.W. Bower, W.J. Mayer, Growth Kinetics Observed in the Formation of Metal Silicides on Silicon, Appl. Phys. Lett. 20 (1972) 359.

[25] S. Prawer, R.J. Nemanich, Raman spectroscopy of diamond and doped diamond, Phil. Trans. R. Soc. Lond. A. 362 (2004) 2537–2565.

[26] V. Mortet, L. Zhang, M. Eckert, J. D'Haen, A. Soltani, M. Moreau, D. Troadec, E. Neyts, J.C. De Jaeger, J. Verbeeck, A. Bogaerts, G. Van Tendeloo, K. Haenen, P. Wagner, Grain size tuning of nanocrystalline chemical vapor deposited diamond by continuous electrical bias growth: Experimental and thoretical study, Phys. Stat. sol. (a) 209 (2012) 1675-1682.

[27] H. Lange, M. Giehler, W. Henrion, F. Fenske, I. Sieber, G. Oertel, Growth and Optical Characterization of $CrSi_2$ Thin Films, Phys. Status Solidi. 63 (1992) 63–76.

[28] H. Nienhaus, T. Kampen, W. Mönch, Phonons in 3C-, 4H-, and 6H-SiC, Surf. Sci. Lett. 324 (1995) 328–332.

[29] J. Xie, J. Shen, N.Chen, S. Seetharaman, Site preference and mechanical properties of $Cr_{23-x}T_2C_6$ (T=Mo,W), Acta. Materialia. 54 (2006) 4653–4658